Nanoscale-Driven Crystal Growth of Hexaferrite Heterostructures for Magnetoelectric Tuning of Microwave Semiconductor Integrated Devices

Bolin Hu,[†] Zhaohui Chen,[†,§] Zhijuan Su,[†] Xian Wang,[†,∥] Andrew Daigle,[†,⊥] Parisa Andalib,[†] Jason Wolf,[‡] Michael E. McHenry,[‡] Yajie Chen,[*,†] and Vincent G. Harris[†]

[†]Center for Microwave Magnetic Materials and Integrated Circuits, and Department of Electrical and Computer Engineering, Northeastern University, Boston, Massachusetts 02115, United States and [‡]Materials Science and Engineering, Carnegie Mellon University, Pittsburgh, Pennsylvania 15213, United States. [§]Present address Z.C.: HGST, San Jose, CA 95135. [∥]Present address X.W.: School of Optical and Electronic Information, Huazhong University of Science and Technology, Wuhan, Hubei 430074, China. [⊥]Present address A.D.: MIT Lincoln Lab, Lexington, MA 02421.

ABSTRACT A nanoscale-driven crystal growth of magnetic hexaferrites was successfully demonstrated at low growth temperatures (25−40% lower than the temperatures required often for crystal growth). This outcome exhibits thermodynamic processes of crystal growth, allowing ease in fabrication of advanced multifunctional materials. Most importantly, the crystal growth technique is considered theoretically and experimentally to be universal and suitable for the growth of a wide range of diverse crystals. In the present experiment, the conical spin structure of Co_2Y ferrite crystals was found to give rise to an intrinsic magnetoelectric effect. Our experiment reveals a remarkable increase in the conical phase transition temperature by ~150 K for Co_2Y ferrite, compared to 5−10 K of Zn_2Y ferrites recently reported. The high quality Co_2Y ferrite crystals, having low microwave loss and magnetoelectricity, were successfully grown on a wide bandgap semiconductor GaN. The demonstration of the nanostructure materials-based "system on a wafer" architecture is a critical milestone to next generation microwave integrated systems. It is also practical that future microwave integrated systems and their magnetic performances could be tuned by an electric field because of the magnetoelectricity of hexaferrites.

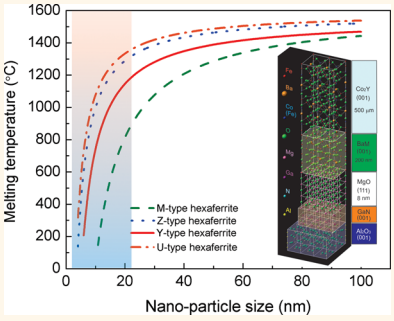

KEYWORDS: magnetoelectric · nanoscale · epitaxial single crystal growth · semiconductor integrated

Hexaferrites (i.e., hexagonal ferrites), discovered in 1950s, exist as any one of six crystallographic structural variants (i.e., M-, X-, Y-, W-, U-, and Z-type). Over the past 6 decades, the hexaferrites have received much attention owing to their important properties that lend use as permanent magnets, magnetic data storage materials, as well as components in electrical devices, particularly those operating at rf frequencies. Moreover, there has been increasing interest in hexaferrites for new fundamental and emerging applications. Among those, electronic components for mobile and wireless communications especially incorporated with semiconductor integrated circuits at microwave frequencies,[1] electromagnetic wave absorbers for electromagnetic compatibility, random-access memory (RAM) and low observable technology, and as composite materials having low dimensions.[2] However, of particular interest is the magnetoelectric (ME) effect discovered recently in the hexaferrites such as $SrScxFe_{12-x}O_{19}$ (SrScM), $Ba_{2-x}Sr_xZn_2Fe_{12}O_{22}$ (Zn_2Y), $Sr_4Co_2Fe_{36}O_{60}$ (Co_2U), and $Sr_3Co_2Fe_{24}O_{41}$ (Co_2Z), demonstrating ferroelectricity induced by the complex internal alignment of magnetic moments.[3] Further, both Co_2Z and Co_2U have revealed observable magnetoelectric effects at room temperature, representing a step toward practical applications using the ME effect. These materials hold great potential for applications, since strong magnetoelectric coupling allows switching of the FE polarization with a magnetic field (H) and vice versa. These features could lead to a new type of storage devices, such as an electric field-controlled magnetic memory.

Both traditional and modern microwave components require hexaferrites due to

* Address correspondence to y.chen@neu.edu.

Received for review May 6, 2014 and accepted October 8, 2014.

Published online October 08, 2014
10.1021/nn504714f

their moderate to high values of magnetization, tunable magnetocrystalline anisotropy field, high permeability, high permittivity, and low-losses at rf frequencies. Additionally, these hexaferrite materials also provide nonreciprocal behavior that is essential for many device applications in radar and communications systems such as in isolators, circulators, *etc*. It is noteworthy that the microwave electronics community has long sought to integrate microwave passive devices, such as circulators, isolators, phase shifters, filters, *etc*. with semiconductor device platforms such as GaN thus allowing for system-on-a-wafer architectures.[4,5] Such an achievement would address the demands of ever increasing systems integration while enhancing performance and functionality and concomitantly reducing device profile,[6] volume, and weight.[7] Previous attempts to integrate ferrite materials onto Si and GaAs failed in that the high temperatures required for the processing of low microwave loss ferrite materials resulted in the degradation of microwave performance. It is clear that a low temperature ferrite growth technique is key to realizing planar microwave semiconductor integrated devices including those ideally tuned by electric fields based on the room temperature magnetoelectric effect.

A novel attempt to integrate single crystal Y-type hexaferrite heterostructures on wideband semiconductor substrates is proposed. We show such structures demonstrate the ME effect allowing for E field tuning at microwave frequencies. Single-crystal Co_2Y, *i.e.*, $Ba_2Co_2Fe_{12}O_{22}$, ferrites are an important class of microwave ferrites that are widely used in microwave and millimeter-wave filters and phase shifters. Wide band gap semiconductor materials, *e.g.*, SiC and GaN,[8,9] have demonstrated advantages in power handling at high frequencies and received great interest from the semiconductor device community due to their attractive thermal conductivities, band gap energies, breakdown voltages, and permittivity, among other properties.[10] Additionally, these materials share the same hexagonal crystal symmetry and comparable lattice parameters as hexagonal ferrites and possess the high temperature stability that enables epitaxial growth of high-quality microwave ferrites.

We propose that the preparation of single crystal Y-type hexaferrite having thicknesses in the 10s or even 100s of micronson lattice mismatched semiconductor substrates is challenging.[11] Since the 1960s, synthesis techniques for the growth of ferrite single crystals include the melt salt method,[12] liquid phase epitaxy (LPE), and floating zone method.[13,14] Among these, either floating zone method or LPE growth involves complicated liquid phase control and expensive experimental setup, while the salt melting method, although simple to execute and scalable, involves long cooling cycles and etching of the crystals out from the crucible. A 4 μm thick Co_2Y ferrite film has been successfully grown on $MgAl_2O_4$ substrate at low temperature,[15] but it is still too thin to be used in many practical devices. The development of low temperature epitaxial ferrite thick films or crystals with low microwave loss remains a problem whose solution will have a wide-ranging impact upon the microwave device community.

In order to realize heteroepitaxial growth, thermal and structural compatibilities of the substrate's surface and the growing film are key factors. Here, we present an innovative solution that employs the use of ferrite nanoparticles to facilitate the growth of large area, *i.e.*, ~1 cm^2 Co_2Y ($Ba_2Co_2Fe_{12}O_{22}$) films with thicknesses ranging from 80 to greater than 500 μm on GaN substrates without the need for an enabling flux. The omission of a flux is attractive in that it often introduces contaminants to the growing films leading to unwanted effects to magnetic and microwave properties. In this experiment, we demonstrate the use of ~20 nm diameter Co_2Y powder positioned atop a GaN/Al_2O_3 substrate to realize epitaxial growth of an 80−500 μm thick film of Co_2Y at temperatures as low as ~1050 to 1150 °C without flux.[16] A GaN/Al_2O_3 substrate was employed with the thickness of GaN of ~30 μm. In the case of Y type ferrite films grown on GaN, there is a relatively large lattice mismatch of 6.2% between the GaN (001) substrate and the Co_2Y (00l) film thus requiring a buffer layer to mediate interfacial strain and realize epitaxial growth. Further complicating growth is that GaN is thermally unstable in vacuum at temperatures near 950 °C at which typical pulsed laser deposition (PLD) growth of ferrite film seeds are grown. In order to mitigate both interfacial strain and surface reactivity, a layer of MgO, having (111) crystallographic orientation, was grown on the GaN substrate. Following the preparation of the MgO (111) buffer layer, $BaFe_{12}O_{19}$ (BaM) was deposited between Co_2Y and MgO.[17] Ultimately, the designed architecture consisted of five layers: (001) sapphire (Al_2O_3), (001) GaN, (111) MgO, (001) BaM, and (001) Co_2Y, as illustrated in Figure 1.

RESULTS AND DISCUSSION

The Co_2Y nanoparticles, synthesized by an aqueous chemical coprecipitation method were examined for crystallographic structure and morphology by X-ray diffraction (XRD) and scanning electron microscopy (SEM), respectively. In Figure 2a, the XRD spectrum collected using Cu Kα radiation at room temperature in a θ-2θ geometry displays a single phase of hexagonal Co_2Y structure, indicating a high crystal quality of nanoparticles.[18] An average grain size of 36 ± 6 nm was calculated using the Scherrer equation, whereas the grain size observed in electron microscopy images range from 10 to 40 nm (Figure 2b). More precise statistical data (Figure 2c) indicate that approximately 70% of the nanoparticles have a grain size in the range

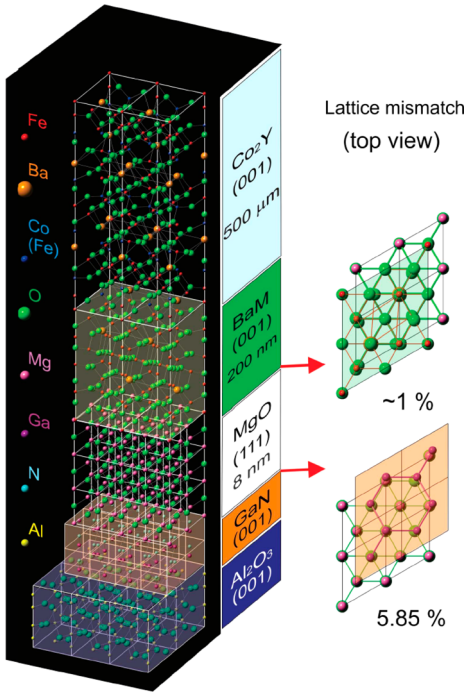

Figure 1. Atom view of the Co_2Y film growth on GaN substrate.

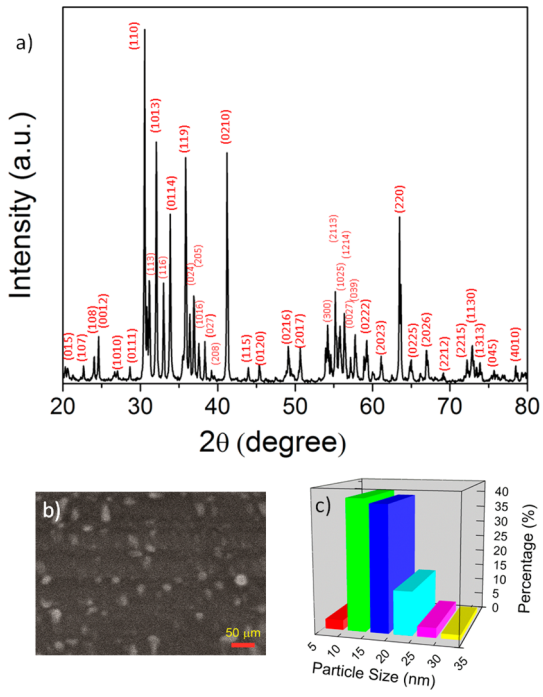

Figure 2. (a) XRD of Co_2Y nano particles; (b) statics bar of the nanoparticles size distribution; (c) SEM image of Co_2Y nanoparticles.

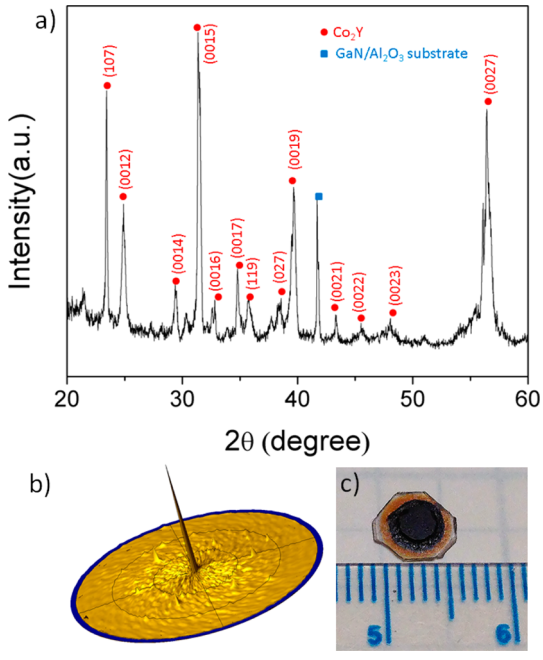

Figure 3. (a) XRD patterns for Co_2Y films grown at 1100 °C. Diffraction peaks have been identified with either the Co_2Y film or the GaN/Al_2O_3 substrate. (b) Pole figures were obtained from the (0027) peak reflections. (c) Real image of the sample with thickness of 500 μm.

of 10−20 nm, which is indeed dominant in the distribution of the particle size. It is assumed to play a crucial role in lowering the melting temperature of the Y-type ferrite powder, which will be discussed later in the theoretical section. Crystal structure and texture of the resulting Co_2Y crystals (shown in Figure 3c),[19] grown at a low temperature of ~1050 °C, were studied by room temperature XRD. The XRD pattern of the Co_2Y thick ferrite film grown on a GaN/Al_2O_3 substrate is illustrated as Figure 3a. It is observed that the Co_2Y phase remains the dominant phase possessing (00*l*) preferred orientation. The peak near 41.6° (in 2θ) corresponds to that of the substrate. Additionally, the peaks at 24.5°, 30.8°, 39.2°, and 57°correspond to (0012), (0015), (0019), (0027) planes of the Co_2Y film, respectively. Lattice constants of the doped Co_2Y were obtained by analysis of the XRD data and resulted in a *c* of 43.62 Å and an *a* of 5.88 Å. These results are consistent with previous published results for the Co_2Y phase.[20] The lattice mismatch between the (111) MgO, ~5.957 Å, BaM, ~5.89 Å, and Co_2Y, ~5.88 Å, crystallographic planes are less than ~1%: this is a critical factor in achieving epitaxial growth. To further characterize the crystal quality of the Co_2Y films, a pole figure was obtained from the (0027) diffraction peak. These data are shown as Figure 3b. In collecting these data, the angle between the film normal and the vector bisecting the incident and detected X-ray beams, φ, was varied from 0° to 90°, and the azimuthal angle about the bisecting vector, ξ, was varied from 0° to 360°. The peak at the center of the (0027) pole figure indicates *c*-axis alignment normal to the film plane with low in-plane dispersion. The 6-fold symmetry of low intensity peaks arise from the (039) Co_2Y planes having similar values in *d* spacing. These results confirm the epitaxial growth of Co_2Y (001) on BaM (00l)/MgO(111)/GaN(001)/Al_2O_3 (001).

The surface morphology of the Co_2Y films was observed in SEM and presented as Figure 4a. Hexagonal

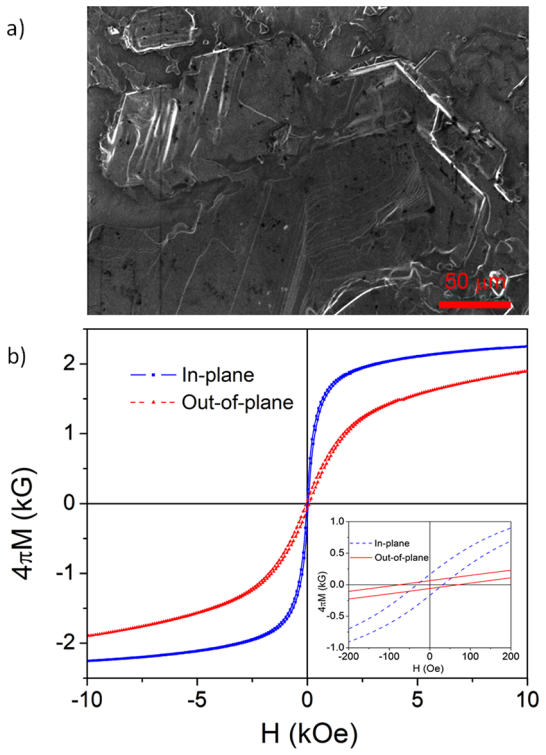

Figure 4. (a) SEM image of the Co_2Y film surface; (b) hysteresis loop of thick Co_2Y ferrite films with in-plane and out-of-plane magnetic field applied. Inset of part b is an enlarged magnetic hysteresis loop at low field.

growth facets are clearly visible on the film surface, confirming the orientation of crystals with the crystallographic *c*-axis aligned normal to the film plane. The chemical composition of the Co_2Y films was determined using energy-dispersive X-ray spectroscopy (EDX). The results indicate a ratio of $BaO/CoO/Fe_2O_3$ is ~1:1:3 in the Co_2Y ferrite films, which confirms that this growth methodology is a relatively simple, cost-effective, and an environmentally friendly (*i.e.*, no toxic flux) method of depositing thick ferrite films with high purity and crystalline quality.[21] The magnetic properties of Co_2Y films were measured using vibrating sample magnetometry (VSM) at room temperature with a magnetic field ranging from −10 kOe to 10 kOe. Both in-plane and out-of-plane hysteresis loops are presented as Figure 4b. It is shown that the hard axis of the Co_2Y film aligns out of the film plane consistent with the crystallographic *c*-axis aligning perpendicular to the sample plane. The hysterias loop collected with the applied magnetic field aligned in the film plane experiences a magnetization ($4\pi M$) of 2.2 ± 0.1 kG at 10 kOe that matches the properties of high quality Co_2Y ferrite.[22] The intrinsic coercivities derived from in-plane and out-of-plane measurements were measured to be 32 and 73 Oe, respectively. Also, an enlarged scale plot of the $M-H$ curve under application of small magnetic fields is presented as the inset to Figure 4b. The Co_2Y crystal is seen to possess large magnetic anisotropy. We propose that the magnetization along the hard-axis (i.e., *c*-axis) consists of two mechanisms as is evidenced by the pronounced inflection in the curve as it approaches saturation. This behavior deviates from the straight-line curve observed in epitaxial films and some reported crystals.[23,24] We assume that the Co_2Y crystals consist of multiple magnetic domains, including nonuniform domains. We conjecture that domain wall motion is initialized at low magnetic fields resulting in high susceptibility (i.e., large slope of the magnetization curve), followed by spin-rotation.[25]

The microwave properties of the Co_2Y thick film samples were measured by ferromagnetic resonance (FMR) as the power derivative as a function of applied magnetic field and plotted as Figure 5a. FMR was measured at a frequency of 9.53 GHz with a peak-to-peak derivative line width of 280 ± 20 Oe for the case where the magnetic field was applied along the plane of the sample. In-plane angular variation was studied and the results indicate the FMR resonance field experiences 6-fold symmetry with a period of 60°. By plotting the magnetic resonant field, H_r, versus the in-plane angle of the external field, φ, (see Figure 5b), it is clear that H_r behaves as a cosine function of φ. Here, $H_r = H_A^{\varphi} \cos 6\varphi$, where we deduced the in-plane anisotropy field H_A^{φ} to be 55 ± 2 Oe. As expected for the Y type hexaferrite, the out-of-plane anisotropy field as H_A^{θ} was found to be substantially larger than H_A^{φ}. The theoretical resonance condition is given by

$$f = \gamma' \sqrt{(H + H_A^{\varphi})(H + H_A^{\varphi} + H_A^{\theta} + 4\pi M_s)} \qquad (1)$$

Here, γ' refers to the effective electron gyromagnetic ratio and its value is 2.8×10^6 Hz/Oe. Substituting the FMR driving frequency and the saturation magnetization into the FMR condition, the out-of-plane magnetocrystalline anisotropy, H_A^{θ}, value was determined to be 32 ± 3 kOe. This value is in good agreement with published results.[26]

The temperature dependence of the zero-field cooled magnetization curve was measured between 5 and 900 K at an applied field strength of 100 Oe along the *c*-axis of the sample,[27] as depicted in Figure 6a. It is observed that the magnetization exhibits four pronounced changes with temperature at 162, 456, 680, and 759 K for the particular ferrite heterostructure studied. It is noticed that the magnetization drops precipitously at ~680 K presumably corresponding to the Curie temperature T_{c1} for the Y type ferrite. It represents a magnetic phase transition from ferrimagnetic (i.e., collinear spins structure) to paramagnetic structure, as the temperature increases beyond T_{c1}. The paramagnetic phase gives rise to very small moments (usually close to zero). However, interestingly, what we observed is that the ferrite heterostructure is still of high magnetization (half the magnetization of Y-type) at $T > T_{c1}$, followed by another precipitous drop in

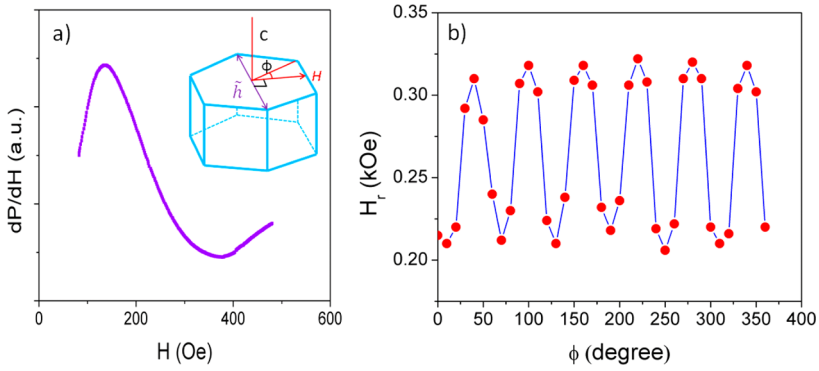

Figure 5. (a) In-plane FMR measurement of thick Co_2Y films at 9.53 GHz and (b) magnetic resonant field H_r plotted as a function of the in-plane angle φ of the external field.

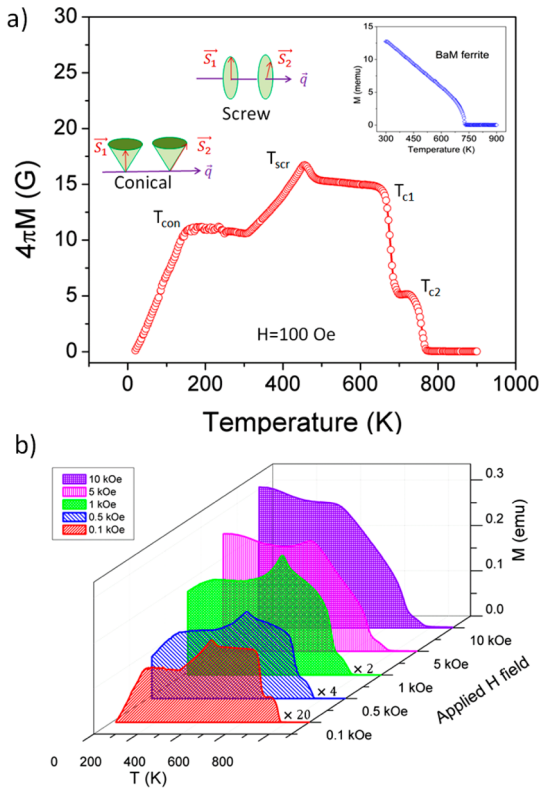

Figure 6. (a) Temperature dependence of magnetization for the Co_2Y crystal at applied magnetic fields along the *c*-axis and over a temperature range from 5 to 1000 K. (a) Applied magnetic field of 100 Oe and (b) applied magnetic fields of 0.1, 0.5, 1.0, 5.0, and 10 kOe.

magnetization to near zero as the temperature rises to ~759 K. The following phase transition is attributed to the Curie temperature, T_{c2}, for the M-type ferrite buffer film in this heterostructure.[22] The *M* vs *T* plot of BaM ferrite was also measured and is shown as the inset to Figure 6a. These data clearly indicate a phase transition (i.e., ferrimagnetism-paramagnetism) at ~730 K (i.e., Curie temperature of BaM). This is evidence that the phase transition of ~759 K observed for a Co_2Y/BaM heterostructure stems from the BaM buffer layer. The increase in Curie temperature of the BaM film in a Co_2Y/BaM heterostructure likely results from an internal interfacial strain as the BaM thin layer is sandwiched between the substrate and the Co_2Y crystal. Thus, it is reasonable that the magnetization between T_{c1} and T_{c2} originates from the ferrimagnetism of the M-type hexaferrite with collinear spin structure. The magnetic signature of the BaM in the *M*−*T* curve is evidence that the thin seed layer of BaM between MgO and Y-type ferrite crystal is well formed without extensive diffusion during growth of the Y-type heterostructure by the nanoparticle-assisted growth technique.

Furthermore, two peaks observed in the *M* vs *T* curve of Figure 6a appear at low temperatures. Previous investigations of Y-type ferrites indicate that ferrimagnetic spin structure may transfer into a proper screw,[28,29] and even conical spin structure, at temperatures much lower than its Curie temperature. In the present work, it is assumed that the phase transition at 456 K corresponds to a spin transition to a screw spin state, in which alternating stacks of magnetic blocks develop a screw rotation with the spin rotation axis parallel to the modulation wave vector $\vec{q}$ (parallel to *c*-axis), whereas the moment $\vec{S}$ in each of the magnetic blocks prefers to lie within the *a*−*b* plane, which was verified by neutron diffraction studies.[21,22] More importantly, as the temperature drops further, the screw phase transforms to a transverse conical structure. The anomaly at 162 K from Figure 6a is likely to reflect a transition from screw to transverse conical spin configurations (named a transverse conical spin temperature T_{con}). The transverse conical structure is of great importance and may result in the observation of a magnetoelectric effect.

Below T_{con} an increase or decrease in net magnetization with decreasing temperature may be observed as the materials remain in a conical spin state. Actually, the temperature dependence of magnetization in conical spin structures is complicated and depends upon both the strength and orientation of the applied magnetic field. Previous work includes a systematic investigation of the dependence of magnetization with temperature under different applied magnetic field strengths.[27] Either enhanced or

suppressed, the magnetization can be measured as the strength of the applied field changes. Only when the temperature is below T_{con} does a nonzero solution to the above equation can be derived from the transverse conical structure. It ultimately may lead to the induced electrical polarization so as to lay the foundation of future ME-based applications. On the basis of previous reports on magnetoelectric effect and conical spin structure,[2] it is predictable that the Co_2Y ferrite crystal demonstrates a magnetoelectric effect at $T < T_{con} = 162$ K, which is a remarkable increase in conical temperature among those Y-type ferrites reported ($T_{con} = 5-10$ K).[30] This increased temperature is associated with introduction of cobalt ion into Y-type ferrite, enhancing magnetocrystalline anisotropy field up to $H_A = 30$ kOe, compared to those Zn or Mg doped Y-type ferrites with $H_A = 10$ kOe.[22] The enhanced temperature of conical structure may lead to the realization of magnetoelectric tuning of real microwave devices. However, it should be pointed out that all of the magnetic phase transitions presented are sensitive to the applied magnetic field, as shown in Figure 6b. Screw and conical structure temperature shift to low temperature as a magnetic field is increased, whereas Curie temperatures for Y- and M-type ferrites increase with increasing field. In particular, a high magnetic field (>1 kOe) may destroy the conical structure leading to the disappearance of the magnetization peak at around 162 K. These new results provide potential to manipulate spin structures in Y-type ferrites having a high temperature of magnetoelectric coupling.

All of the measurements discussed above indicate the novel crystal growth of high-quality Co_2Y hexaferrite that was accomplished at low temperatures assisted by the high surface area to volume ratio of nanoparticles. The nanoscale-driven crystal growth is of significance in both fundamental research and engineering applications. In this work, it is understandable that the reduced melting temperature of the nanoparticles is attributed to its small particle size with high surface energy. The relationship between melting temperature and particle size can be quantitatively calculated in terms of eq 2. This dependence of melting upon particle size is not restricted to any particular material; rather, it encompasses a wide variety of materials from metals to semiconductors and to molecular organic crystals.[31]

$$\frac{T_m(r)}{T_m(\infty)} = 1 - \frac{4}{\rho_s L}\left[\gamma_s - \gamma_l\left(\frac{\rho_s}{\rho_l}\right)^{2/3}\right]\frac{1}{d} \qquad (2)$$

Here, T_m, d, and L are melting temperature, particle diameter, and molar heat of fusion, respectively. γ is the specific surface free energy of the solid (s) or liquid (l). ∞ signifies the bulk material and ρ is density. For ρ_s, it could be obtained from eq 3 and eq 4.[32]

$$V_{cell} = \frac{\sqrt{3}}{2}a^2c \qquad (3)$$

$$\rho_s = \frac{ZM}{N_A V_{cell}} \qquad (4)$$

The lattice constants a and c are 5.88 and 43.62 Å, respectively, derived from XRD analysis, and V_{cell} is the cell volume, M is the molar mass, N_A is Avogadro's number, Z is the number of molecules per unit cell ($Z = 6$ for Y-type hexaferrite). The calculated ρ_s for our sample is ~5.3 g/cm^3, which is close to the reported value.[16] The surface energy of solid ferrite can be estimated from eq 5.[33]

$$\gamma_s = \frac{Eh^2}{\pi^2 d} \qquad (5)$$

E refers here to the elastic constant normal to the (hkl) plane of the crystal structure, which can be estimated by the elastic wave velocity and strain matrix.[34] For the particular case of a hexagonal structure,[35] the expression of E can be obtained from the elastic wave in the longitudinal direction of the (001) plane, *i.e.*, $E_{(001)} = C_{33}$, whereas $C_{33} = C_{11}$ if considering an elastically isotropic hexagonal crystal.[36] Taking a value of $C_{11} \sim 2.825 \times 10^{12}$ dym/cm^2 for a typical ferrite,[22] an elastic constant $E_{(001)}$ for the Y-type hexaferrite exhibits the same order of magnitude as the reported elastic constant for hexagonal ferrites.[37] Next, h is the smallest possible interlayer spacing that could be obtained from the Y-type crystal structure,[38] as illustrated in Figure 7b. Along the ⟨001⟩ directions, the Y-type hexaferrite can be considered to consist of a 18-layer stacking of cations and anions with an interlayer spacing of h (001) = c/18. The periodicity d as the separation between two successive stoichiometric blocks is $d_{(001)} = c$. Thus, the surface energy is derived $\gamma_s \sim 379$ erg/cm^2 from eq 5, which is comparable to other ferrites.[22]

Finally, we estimate a melting temperature of ~1120 °C for the Y-type hexaferrite nanoparticles by taking the parameters: $\gamma_l = 311.6$ erg/cm^2 based on a ratio (1.15−1.2) of γ_s to γ_l,[39] $\rho_s/\rho_l \sim 1.1-1.2$,[40] $T_m(\infty) \sim$ 1550 °C for bulk Co_2Y,[16] $L \sim 1594.6$ cal/mol,[41] and the particle size, $d = 20$ nm for the nanopowders used in this experiment. The predicted melting temperature for the studied hexaferrite nanoparticle is fully consistent with the experimental observation, as depicted in Figure 7a. It should be pointed out that the nanoscale-driven crystal growth technique is of universal significance in lowering the temperature crystal growth for other ceramics or alloys.

As mentioned earlier, such low temperature crystal growth driven by nanoparticles is not restricted to Y-type hexaeferrites or other ferrites. This new technique is available for a wide range of ceramics. Figure 7a presents the predictions of melting temperatures

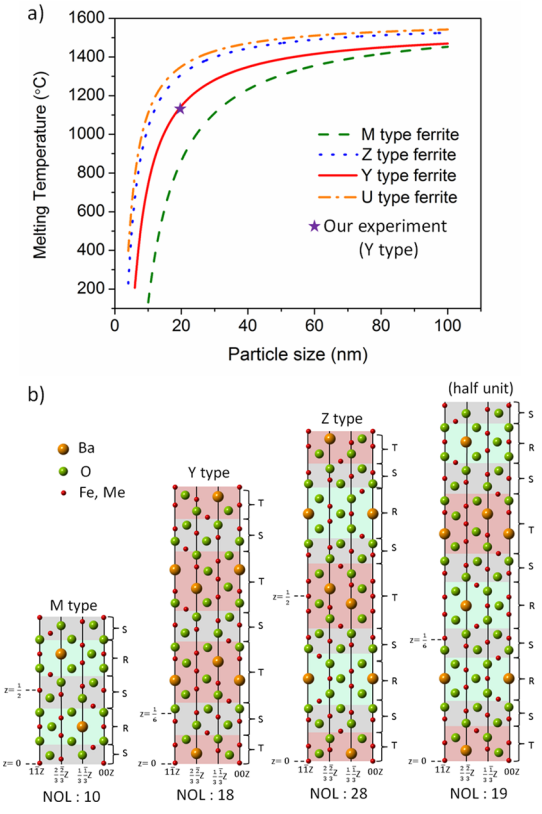

Figure 7. (a) Predictions of melting temperatures varying with particle size for four types of the hexaferrites showing magnetoelectric effects and (b) M-type, Y-type, U-type, and Z-type hexaferrites with different numbers of the oxygen ion layer along the (001) direction in a unit cell.

varying with particle size for four types of hexaferrites that show the magnetoelectric effect and potential for applications in ME-based microwave or other electronic devices. The relationship between melting temperature and particle size is predicted for M-, Y-, U-, and Z-type hexaferrites with different numbers of the oxygen ion layers along the ⟨001⟩ direction in a unit cell, as illustrated in the inset to Figure 7b. It is promising that Z-type hexaferrites can be grown at a relatively low temperature, *i.e.*, <1000 °C, for the case when the enhancing nanoparticle size is less than 15 nm. This could overcome a longstanding limitation in Z-type ferrite crystals that must be grown at extremely high temperatures. As a result, crystal growth temperatures are anticipated to be lowered 20−30% if nanoparticle size is controlled below 20 nm for most ferrites.

CONCLUSIONS

In summary, we have demonstrated a technique for the low-temperature crystal growth of ferrites and other ceramics. Nanoparticles are used to achieve high-quality ferrite crystals grown at temperatures ∼30% lower than conventional growth temperatures without the need for flux. More importantly, this work has demonstrated a unique hexaferrite heterostructure featuring an integration of a magnetoelectric microwave ferrite and wideband semiconductor. The ferrite heterostructure with five layers: Co_2Y hexaferrite/BaM hexaferrite/MgO/GaN/sapphire, was constructed by nanoscale-driven crystal growth technique combined with the pulsed laser deposition technique. These experiments indicate that high-quality Y-type ferrite crystals with thicknesses greater than 500 μm were grown on a wideband semiconductor GaN, showing high crystallographic texture and a low ferromagnetic resonance line width at the X-band. More importantly, the Co-doped Y-type ferrite crystals reveal a conical spin structure at a relatively high temperature of 162 K and have potential to be further modified in temperature. These demonstrations allow the realization of the integration of high-performance *E*-field tunable ferrite microwave passive devices with active circuit elements on a common semiconductor substrate: a necessary step in creating "systems-on-a-wafer" architectures.

METHODS

Synthesis of Co_2Y Nanoparticles (Co_2Y-NPs). The $Ba_2Co_2Fe_{12}O_{22}$ (Co_2Y) nanoparticles were prepared by an aqueous chemical coprecipitation method.[42] Starting powders of $BaCl_2$, Fe(III)Cl_3, $CoCl_2$, NaOH, and Na_2CO_3 were mixed in the appropriate stoichiometric ratios and then were diluted in deionized water independently in 400 mL beakers, after which they were added simultaneously to a larger vessel, which was heated to 951 °C and subsequently mixed using a motorized stirrer at 150 rpm for 2 h. Tetra-ethylene glycol was added during the mixing process to serve as a surfactant, which aided in particle formation. After precipitation, the resultant powders were filtered utilizing vacuum filtration to remove water and NaCl. These precipitated particles then underwent additional rinsing, including ultrasonic vibration and magnetic stirring before subsequently being vacuum filtered and dried. The dried powders were subsequently sintered at 900 °C for 14 h and then was ball milled with alcohol for 20 h to reduce the size after synthesis.

Fabrication of Co_2Y Hexaferrite/BaM Hexaferrite/MgO/GaN/Sapphire Heterostructure. A commercial (001)GaN/(001)Al_2O_3 substrate (Supplied by MTI) was employed with an area of 10 × 10 mm^2, having thicknesses of 30 μm and 0.5 mm for GaN and Al_2O_3, respectively. It is noticed that there is not only a relatively large lattice mismatch of 6.2% between the GaN (001) substrate and the Co_2Y (00l) film, but also GaN is thermally unstable in vacuum at high temperatures near 950 °C at which typical PLD growth of seeded ferrite films was employed. Thus, in order to mitigate both interfacial strain and surface reactivity, an 8 nm layer of MgO, having (111) crystallographic orientation, was deposited at 550 °C by PLD on the GaN substrate prior to the growth. Following the preparation of the MgO (111) buffer layer, a $BaFe_{12}O_{19}$ (BaM) seed layer with a thickness of ∼200 nm was ablated at 900 °C from a homogeneous BaM target within the same chamber without disrupting the vacuum. A KrF excimer laser of wavelength 248 nm operating at 250 mJ per pulse was used in pulsed laser deposition. An oxygen pressure of 20 mTorr, with a corresponding substrate temperature of 900 °C, was determined to be optimal based upon the structure, magnetic, and microwave characterization. Finally, an alumina ring with an inner diameter of 6 mm was placed atop the

substrate and filled with the nanoparticulate Co_2Y powder and placed into a box furnace and heated to 1050−1150 °C, which was shown to result in the melting of the powder. Ramping and cooling rate are at 5 °C/min and 1−3 °C/min, respectively. The Co_2Y crystals have a thickness ranging from 80−500 μm, depending upon the loading factor of the nanoparticles and growth processing.

Characterizations. Crystal structure and texture of the Co_2Y nanoparticles and the resulting Co_2Y crystals grown on GaN were studied by room temperature XRD using Cu Kα radiation in a θ-2θ geometry. The chemical composition of the Co_2Y films was determined using EDX. The magnetic properties of Co_2Y films were measured using VSM at room temperature with a magnetic field strength ranging from −10 kOe to 10 kOe. The microwave properties were measured by ferromagnetic resonance (FMR) as the power derivative as a function of applied magnetic field. Temperature dependences of magnetization were measured by the Quantum Design-Physical Property Measurement System (PPMS) over a temperature range from 5 to 1000 K.

Conflict of Interest: The authors declare no competing financial interest.

REFERENCES AND NOTES

1. Chen, Z.; Yang, A.; Mahalingam, K.; Averett, K. L.; Gao, J.; Brown, G. J.; Vittoria, C.; Harris, V. G. Structure, Magnetic, and Microwave Properties of Thick Ba-Hexaferrite Films Epitaxially Grown on GaN/Al2O3 Substrates. *Appl. Phys. Lett.* **2010**, *96*, 242502.
2. Kimura, T. Magnetoelectric Hexaferrites. *Annu. Rev. Condens. Matter Phys.* **2012**, *3*, 93–110.
3. Ma, J.; Hu, J.; Li, Z.; Nan, C. Recent Progress in Multiferroic Magnetoelectric Composites: from Bulk to Thin Films. *Adv. Mater.* **2011**, *23*, 1062–1087.
4. Harris, V. G. Modern Microwave Ferrites. *IEEE Trans. Magn.* **2012**, *48*, 1075–1104.
5. Zhang, L.; Su, X.; Chen, Y.; Li, Q.; Harris, V. G. Radio-Frequency Magnetron Sputter-Deposited Barium Hexaferrite Films on Pt-coated Si Substrates Suitable for Microwave Applications. *Scripta Mater.* **2010**, *63*, 492–495.
6. Gutfleisch, O.; Willard, M.; Brück, E.; Chen, C.; Sankar, S.; Liu, J. Magnetic Materials and Devices for the 21st Century: Stronger, Lighter, and More Energy Efficient. *Adv. Mater.* **2011**, *23*, 821–842.
7. Harris, V. G.; Geiler, A.; Chen, Y.; Yoon, S.; Wu, M.; Yang, A.; Chen, Z.; He, P.; Parimi, P. V.; Zuo, X.; *et al.* Recent Advances in Processing and Applications of Microwave Ferrites. *J. Magn. Magn. Mater.* **2009**, *321*, 2035–2047.
8. Chen, Z.; Yang, A.; Geiler, A.; Harris, V. G.; Vittoria, C. Epitaxial Growth of M-type Ba-Hexaferrite Films on MgO (111)//SiC (0001) with Low Ferromagnetic Resonance Linewidths. *Appl. Phys. Lett.* **2007**, *91*, 182505.
9. Dietl, T. A Ten-Year Perspective on Dilute Magnetic Semiconductors and Oxides. *Nat. Mater.* **2010**, *9*, 965–974.
10. Huang, Y.; Duan, X.; Cui, Y.; Liebe, C. M. Gallium Nitride Nanowire Nanodevices. *Nano Lett.* **2002**, *2* (2), 101–104.
11. Hu, B.; Chen, Y.; Gillette, S.; Su, Z.; Wolf, J.; McHenry, M.; Harris, V. G. High Quality Y-Type Hexaferrite Thick Films for Microwave Applications by an Economical and Environmentally Benign Crystal Growth Technique. *Appl. Phys. Lett.* **2014**, *104*, 072411.
12. Gambino, R. J.; Leonhard, F. Growth of Barium Ferrite Single Crystal. *J. Am. Ceram. Soc.* **1961**, *44*, 221–224.
13. Glass, H.; Liaw, J. Growth and characterization of LPE hexagonal ferrites. *J. Appl. Phys.* **1978**, *49*, 1578–1581.
14. Akashi, T.; Matumi, K.; Okada, T.; Mizutanil, T. Preparation of Ferrite Single Crystals by New Floating Zone Technique. *IEEE Trans. Magn.* **1969**, *5*, 285–289.
15. Ueno, K.; Ohkubo, I.; Matsumoto, Y.; Okazaki, N.; Hasegawa, T.; Itaka, K.; Koinuma, H. Characterization of Magnetic and Dielectric Properties on Y-Type Magnetoplumbite Epitaxial Thin Films for High Frequency Application. *MRS Proc.* **2001**, *700*, S2–10.
16. Hu, B.; Su, Z.; Bennett, S.; Chen, Y.; Harris, V. G. Epitaxial Growth of 100-m Thick M-Type Hexaferrite Crystals on Wide Bandgap Semiconductor GaN/Al_2O_3 Substrates. *J. Appl. Phys.* **2014**, *115*, 17A513.
17. Hu, B.; Chen, Y.; Su, Z.; Bennett, S.; Burns, L.; Uddin, G.; Ziemer, K.; Harris, V. G. Magnetocrystalline Anisotropy and FMR Linewidth of Zr and Zn-Doped Ba-Hexaferrite Films Grown on MgO (111). *IEEE Trans. Magn.* **2013**, *49*, 7.
18. Hirose, S.; Haruki, K.; Ando, A.; Kimura, T. Mutual Control of Magnetization and Electrical Polarization by Electric and Magnetic Fields at Room Temperature in Y-type BaSr$Co_{2x}Zn_xFe_{11}AlO_{22}$ ceramics. *Appl. Phys. Lett.* **2014**, *104*, 022907.
19. Hovis, D. B.; Faber, K. T. Textured microstructures in barium hexaferrite by magnetic field assisted gelcasting and templated grain growth. *Scripta Mater.* **2001**, *44*, 2525–2529.
20. Vinnik, M. A. Phase Relations in the BaO−CoO−Fe_2O_3 System. *Zh. Neorg. Khim.* **1965**, *10*, 2137–2144.
21. Hibst, H. Hexagonal Ferrites from Melts and Aqueous Solutions, Magnetic Recording Materials. *Angew. Chem.* **1982**, *4*, 270–282.
22. Smit, J.; Wijn, H. P. J. *Ferrrites*; John Wiley & Sons: New York, 1959.
23. Jalli, J.; Bae, S.; Lee, J. J.; Abo, G. S.; Park, J. H.; Mewes, T.; Choi, B. C.; Kim, S. G.; Hong, Y. K. Ferrimagnetic $Sr_{1.5}Ba0.5Zn_2Fe_{12}O_{22}$ (Zn-Y) Single Crystal with Planar Anisotropy. *IEEE Magn. Lett.* **2011**, *2*, 5000104.
24. Jalli, J.; Hong, Y.; Bae, S.; Lee, J.; Abo, G. S.; Park, J.; Choi, B.; Mewes, T.; Kim, S.; Gee, S.; Nam, I.; Tanaka, T. Magnetic and Microwave Properties of Ferrimagnetic Zr-Substituted $Ba_2Zn_2Fe_{12}O_{22}$ (Zn-Y) Single Crystals. *J. Appl. Phys.* **2011**, *109*, 07A509.
25. Bertotti, G. *Hystersis in Magnetism*; Academic Press: San Diego, CA, 1998.
26. Buffler, C. R. Resonance Properties of Single Crystal Hexagonal Ferrites. *J. Appl. Phys.* **1962**, *33*, 1360–1362.
27. Sagayama, H.; Taniguchi, K.; Abe, N.; Arima, T.; Nishikawa, Y.; Yano, S.; Kousaka, Y.; Akimitsu, J.; Matsuura, M.; Hirota, K. Two Distinct Ferroelectric Phases in the Multiferroic Y-Type Hexaferrite $Ba_2Mg_2Fe_{12}O_{22}$. *Phys. Rev. B* **2009**, *80*, 180419(R).
28. Momozawa, N.; Yamaguchi, Y.; Mita, M. Magnetic Structure Change in $Ba_2Mg_2Fe_{12}O_{22}$. *J. Phys. Soc. Jpn.* **1986**, *55*, 1350–1358.
29. Momozawa, N.; Nagano, Y.; Utsumi, S.; Abe, M.; Yamaguchi, Y. Cation Distribution and Helimagnetic Structure of the $Ba_2(Zn_{1-x}Mg_x)_2Fe_{12}O_{22}$System as Revealed by Magnetization Measurements and Neutron Diffraction. *J. Phys. Soc. Jpn.* **2001**, *70*, 2724–2732.
30. Kimura, T.; Tokura, Y. Magnetoelectric Phase Control in a Magnetic System Showing Cycloidal/Conical Spin Order. *J. Phys.: Condens. Matter* **2008**, *20*, 434204.
31. Dick, K.; Dhanasekaran, T.; Zhang, Z.; Meisel, D. Size-Dependent Melting of Silica-Encapsulated Gold Nanoparticles. *J. Am. Chem. Soc.* **2002**, *124*, 2312–2317.
32. Xua, J.; Ji, G.; Zou, H.; Zhou, Y.; Gan, S. Structural, Dielectric and Magnetic Properties of Nd-Doped Co_2Z-Type Hexaferrites. *J. Alloys Compd.* **2011**, *509*, 4290–4294.
33. Mishra, R.; Thomas, G. Surface Energy of Spinel. *J. Appl. Phys.* **1977**, *48*, 4576–4580.
34. Kittel, C. *Introduction to Solid State Physics*, 8th ed.; Wiley: Hoboken, NJ, 2005.
35. Cline, C.; Dunegan, H.; Henderson, G. Elastic Constants of Hexagonal BeO, ZnS, and CdSe. *J. Appl. Phys.* **1967**, *38*, 1944–1948.
36. Ledbetter, H. Elastic Properties of Zinc: A Compilation and a Review. *J. Phys. Chem. Ref. Data.* **1977**, *6*, 1181–1203.
37. Purushotham, Y. *Mod. Phys. Lett. B* **1999**, *13*, 991.
38. Orlov, I.; Palatinus, L.; Arakcheeva, A.; Chapuis, G. Hexagonal Ferrites: A Unified Model of the (TS)*n*T Series in Superspace. *Acta Crystallogr.* **2007**, *B63*, 703–712.
39. Rhee, S. Critical Surface Energies of Al_2O_3 and Graphite. *J. Am. Ceram. Soc.* **1972**, *55*, 300–303.
40. Courtial, P.; Dingwell, D. Densities of Melts in the CaO-MgO-Al_2O_3-SiO_2 system. *Am. Mineral.* **1999**, *84*, 465–476.

41. Bonnickson, K. High Temperature Heat Contents of Calcium and Magnesium Ferrites. *J. Am. Chem. Soc.* **1954**, *76*, 1480–1482.
42. Daigle, A.; DuPré, E.; Geiler, A.; Chen, Y.; Parimi, P. V.; Vittoria, C.; Harris, V. G. Preparation and Characterization of Pure-Phase Co_2Y Ferrite Powders via a Scalable Aqueous Coprecipitation Method. *J. Am. Ceram. Soc.* **2010**, *93*, 2994–2997.